JOURNAL OF Applied Polymer SCIENCE

Influence of hydroxyapatite and BMP-2 on bioactivity and bone tissue formation ability of electrospun PLLA nanofibers

Xiaozhan Yang,[1] Zhensheng Li[2]

[1]School of Optoelectronic Information, Chongqing University of Technology, Chongqing 400054, China
[2]College of Biomedical Engineering, Third Military Medical University, Chongqing 400038, China
Correspondence to: Z. Li (E-mail: li.zhensheng@163.com)

ABSTRACT: An excellent bioactive scaffold material which could induce and promote new bone formation is essential in the bone repair field. In this study, the bioactive material hydroxyapatite (HA) and the bone morphogenetic protein-2 (BMP-2) were added to poly-l-lactic acid (PLLA) using the electrospinning method. Scanning electron microscopy investigations performed on four different fiber scaffolds, PLLA, PLLA/HA, PLLA/BMP-2 and PLLA/HA/BMP-2, revealed that the fibers of all scaffolds are closely interwoven, and the presence of large interconnected voids between the fibers, resulting in a three-dimensional porous network structure that was similar to the structure of the extracellular matrix of healthy bones. In the MG63 cell culture growth experiments, the composite scaffold material PLLA/HA/BMP-2 showed a higher bioactivity than the other three scaffold materials. The four scaffold materials were implanted in rabbits' tibia for 30 and 90 days. The results of the animal experiments indicate that the capability of the PLLA/HA/BMP-2 composite to induce and promote bone tissue formation was better compared with PLLA/HA or PLLA/BMP-2, suggesting that PLLA combined with HA/BMP-2 is a promising material for bone tissue repair. © 2015 Wiley Periodicals, Inc. J. Appl. Polym. Sci. **2015**, *132*, 42249.

KEYWORDS: bioengineering; biomaterials; biomedical applications; fibers

Received 24 December 2014; accepted 19 March 2015
DOI: 10.1002/app.42249

INTRODUCTION

Surgical reconstruction of bone defects caused by injury or tumor resection is usually treated with functional graft materials whose biodegradability and ability to induce and promote the formation of new bone material at the grafted sites are the prerequisites for a successful application.[1,2] Calcium and phosphate ions and mesenchymal stem cells (MSCs) are present at the site of bone defects, which are very important for bone rebuilding. Tissue engineering scaffold materials should therefore utilize the calcium and phosphate ions and MSCs to promote bone reconstruction. The scaffold material should ideally support growth factors as well as cells.[3–5] To achieve this effect, a scaffold must be three-dimensional and porous, mimicking the extracellular matrix (ECM) of healthy bones.[6–8]

Scaffolds based on nanofibers offer great advantages, and, compared to solid-wall structures, their nanofibrous architecture may serve as a superior scaffold concerning the promotion of osteoblast differentiation and biomineralization.[2,9–11] Electrospinning is a simple and promising method for the fabrication of continuous fibers. A nanofiber scaffold produced by electrospinning could be used to simulate the ECM to support cell breeding and differentiation.[12–15]

As reported in literature, poly-l-lactic acid (PLLA) plays an important role in biomaterials due to its biocompatibility, biodegradability and FDA approval, allowing its application in bone reconstructive surgery.[16,17] PLLA can easily be obtained by electrospinning, resulting in a three-dimensional and porous tissue engineering scaffold. Furthermore, stem cells seem to grow well on PLLA nanofiber scaffolds.

Hydroxyapatite (HA), a bone-like apatite, is a bioactive material. During bone repair or bone reconstruction, the HA particles can act as nucleation centers and promote the deposition of calcium and phosphate ions, and thus accelerate biomineralization and new bone rebuilding.[18–20] The bone morphogenetic protein-2 (BMP-2), which has been shown to induce MSCs to differentiate into osteoblasts in order to promote osteoblast mineralization, has been successfully applied in a number of clinical studies for the reconstruction of bone defects. BMP-2 can also be incorporated into nanofiber scaffolds in a bioactive form by electrospinning.[21–24]

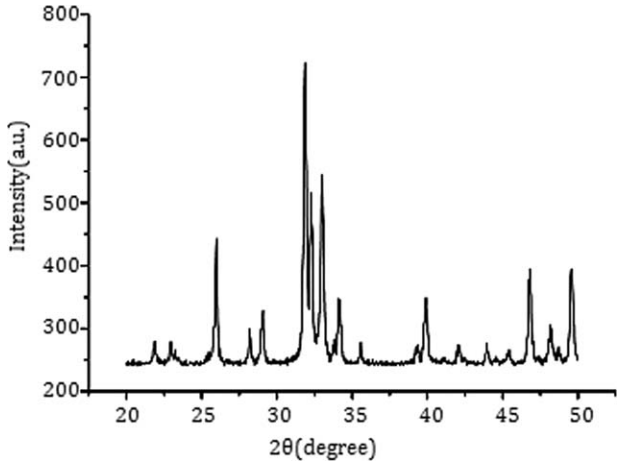

Figure 1. XRD pattern obtained for the as-prepared HA.

In this study, BMP-2 and HA were embedded into the biodegradable polymer PLLA to prepare tissue engineering scaffold materials that simulate the structure of ECM. We aimed to produce functional bone repair scaffolds, which utilize sources such as calcium and phosphate ions, and the MSCs of bone defects to improve bone reconstruction.

MATERIALS AND METHODS

Sample Preparation

The PLLA used in the experiments was purchased from Jinan Daigang Biomaterial Co. Ltd., China, and BMP-2 was purchased from Cyagen, Guangdong, China. The HA powder was synthesized in our lab with the wet method. The XRD analysis (TF-XRD, X'pert Pro MPD, Philips, Netherlands) showed that the HA was pure (cp. Figure 1). The size of the HA powder particles was 55 ± 11 nm (cp. Figure 2, Zetasizer Nano ZS, Malvern, United Kingdom).

The solution of 7 wt % PLLA in choroform was prepared by directly adding the PLLA to the chloroform. After resting for 24 h at room temperature, homogeneous solutions were obtained. The HA (1 wt %), BMP-2 (62.5 μg/mL), and HA (1 wt %)/BMP-2 (62.5 μg/mL) were added to the homogeneous PLLA chloroform solution, respectively. These three mixed solutions were then stirred for 30 min.

Nanofiber Fabrication by Electrospinning

Four different solution systems were prepared. In order to obtain continuous and uniform nanofibers, during the production process of the four scaffold materials, the parameters (cp. Table I) of the electrospinning process were slightly adjusted. A flow rate of 0.6–0.7 mL/h was maintained using a syringe pump. The voltage was in the range from 12 to 14 kV. The electrospun fibers were collected on a collection screen, with a distance between the capillary tube and the collection screen of 15 cm. For this spinneret, the inner capillary diameter was 0.4 mm.

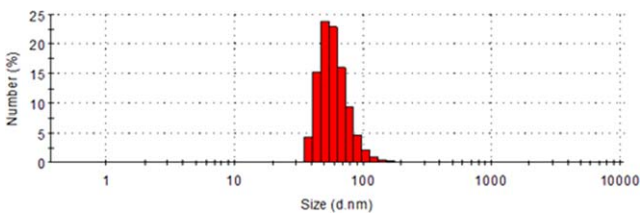

Figure 2. Particle size scattergram obtained for the HA powder particles. The average HA particle size was 55 ± 11 nm. [Color figure can be viewed in the online issue, which is available at wileyonlinelibrary.com.]

Table I. Comparison of the Parameters Used for the Electrospinning for the Four Different PLLA Scaffold Materials

Samples	Voltage (kV)	Distance (cm)	Flow rate (mL/h)
PLLA	12	15	0.7
PLLA/HA	12	15	0.7
PLLA/BMP-2	13.5	15	0.6
PLLA/HA/BMP-2	13.5	15	0.7

The morphology of the four different scaffolds was observed by scanning electron microscopy (SEM, JSW-5900LV-JEOL). The surface area of the scaffolds was determined using standard Brunaner Emmett-Teller (BET) analyzer (ASAP 2020). The scaffolds porosity was measured using the method reported in the literature.[25] According to literature, the surface energy of materials is correlated to its bioactivity.[26] The contact angles of the four scaffold materials were measured using a contact measurement instrument (KSV CAM 200). Then, the surface energies were obtained from the contact angles.[27]

Cell Cultures

The four scaffold materials were distributed into 24 multi-well plates to grow cell cultures and thereby test the biocompatibility of the materials. One milliliter of the human osteosarcoma cell line, MG63, diluted in DMEM (Dulbecco's modified Eagle's medium) supplemented with a 10% fetal bovine serum, was seeded into each well at a density of 3×10^3 cells/mL, and exposed to a 5% CO_2 environment at 37°C for 2, 4, and 6 days, respectively. The medium was changed every 2 days.

MTT Assay

At the end of the designated time periods, 0.2 mL of a MTT [3-(4, 5-dimethylthiazol-2-yl)-2, 5-diphenyltetrazolium bromide] solution (5 mg/mL in DMEM) were added into each well. Afterwards, the cells were further cultured for 4 h, and then the plates were washed with a phosphate buffer saline (PBS) twice. Next, 0.6 mL dimethyl sulfoxide was added into each well. After the wells were shaken for 10 min, the mixed solution of each well was transferred into 96 multi-well plates. The optical densities (OD) were recorded at 490 nm (Bio-Rad iMark, USA).

SEM Analysis

The morphology of the MG63 cells on the four scaffold materials was examined by SEM. After 4 days, the substrates were washed with PBS twice. The cells were then fixed with a 2.5% glutaraldehyde buffer for 24 h at 4°C, and then sequentially dehydrated in increasing concentrations of ethanol. The samples

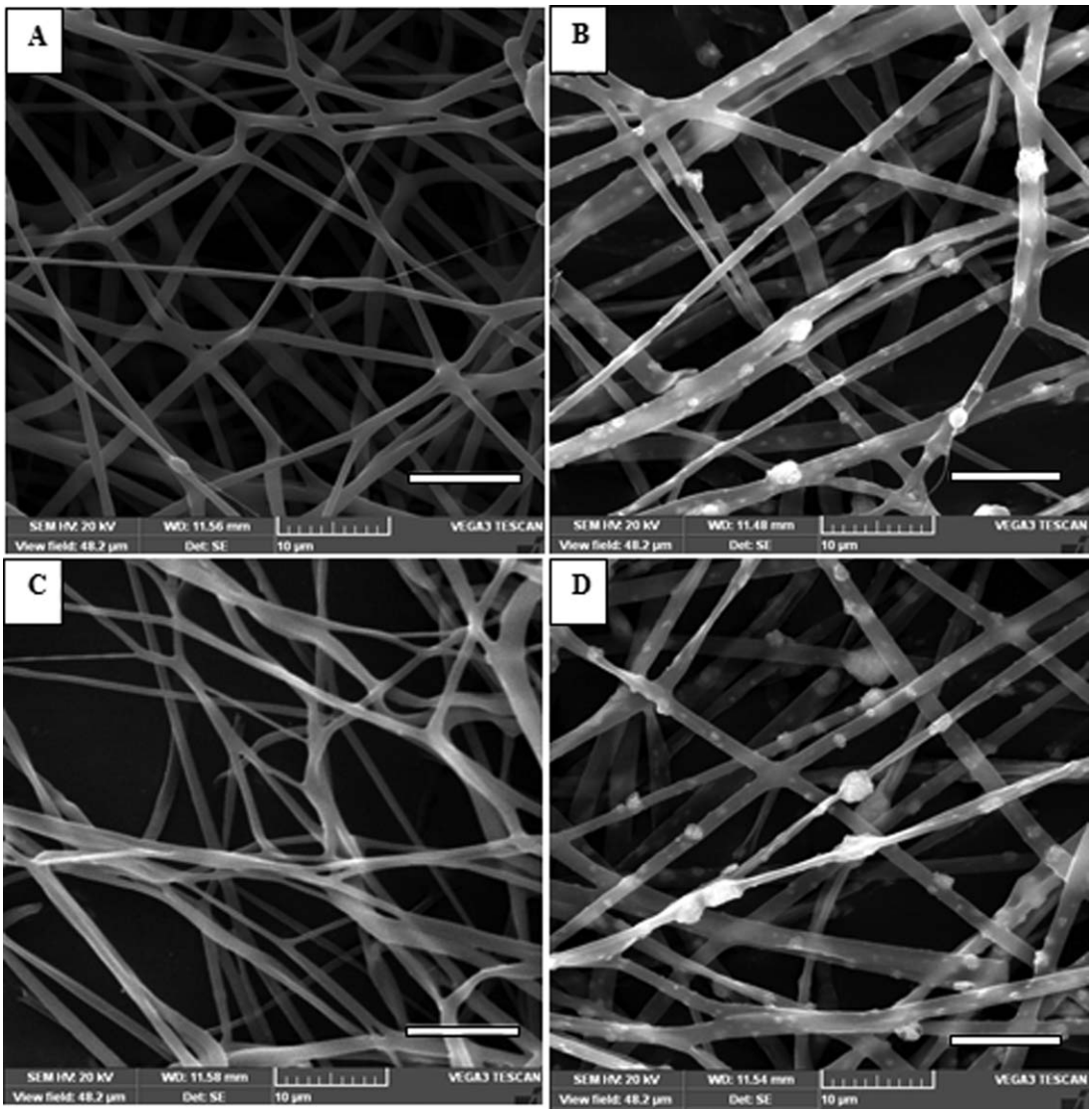

Figure 3. Representative SEM micrographs of the four scaffold materials. (A) PLLA; (B) PLLA/HA; (C) PLLA/BMP-2; (D) PLLA/HA/BMP-2. Scale bar = 10 μm.

were subjected to critical desiccating, followed by gold coating for the SEM observations.

Animal Experiments

Implanted Materials. Eight rabbits with a weight of approx. 3 kg each were used as animal model and divided into two groups. The rabbits in the first group were treated with PLLA and PLLA/HA in the left and right tibia bone, respectively. The second group of rabbits was treated with PLLA/BMP-2 and PLLA/HA/BMP-2 in the left and right tibia bone, respectively.

All operations were performed under general anesthesia by intravenous injection of a mixture of ketamine hydrochloride (40 mg/kg) and xylazine (10 mg/kg). One drill-hole defect with a diameter of 3 mm was created in the left and right tibia of each rabbit. Four samples, PLLA, PLLA/HA, PLLA/BMP-2 and PLLA/HA/BMP-2, were planted into each tibia bone. The rabbits received a penicillin injection for 7 days to prevent infection. The rabbits were raised for 30 and 90 days.

Tissue Section Analysis. Animal sacrifice was performed after anesthesia after 30 or 90 days, respectively. The bone tissue samples were then retrieved and fixed with a 10% neutral buffer formaldehyde solution for 3 days. Then, the fixed solution was changed into a mixed solution of the 10% neutral buffer formaldehyde solution and a 6% nitric acid solution for decalcification for 3 days. The samples were embedded in paraffin and then cut into thin films with a thickness of about 10 μm with histotome. All films were dyed with HE stain prior to the inverted microscope analysis.

RESULTS

Fiber Structure

Representative SEM micrographs of the four electrospun nanofiber scaffolds are shown in Figure 3. In all scaffolds, the fibers are closely interwoven and there are large interconnected voids between the fibers, resulting in a three-dimensional porous

Table II. The Morphological Parameters of the Four Different PLLA Scaffold Materials

Specimens	Average diameter (nm)	Porosity (%)	BET surface area (m^2/g)
PLLA	753 ± 61	81 ± 5	18.3278
PLLA/HA	809 ± 42	85 ± 7	27.0938
PLLA/BMP-2	784 ± 51	82 ± 4	22.0782
PLLA/HA/BMP-2	832 ± 67	83 ± 6	29.6579

network structure, similar to the structure of ECM. The micrographs also revealed that the additive BMP-2 [Figure 3(B,D)] did not change the morphology of the scaffold fibers. In contrast, the additive HA significantly changed the morphology of the membrane materials. Furthermore, the micrographs revealed that HA nanoparticles are uniformly distributed in the nanofibers and there are a number of HA nanoparticles protruding the surface of the nanofibers. These protruding HA nanoparticles might act as nucleation centers and promote the deposition of calcium and phosphate ions and thus accelerate biomineralization. The average diameter, the porosity, and the BET surface area of the four scaffolds were showed in Table II.

Contact Angle and Surface Energy

That first comes into contact with a living body is the surface of a scaffold. Hence, the initial response of cells to the biomaterial, such as cell adhesion, proliferation, migration, and differentiation, mostly depends on the surface properties of the scaffolds. A higher surface energy makes atoms on the surface more active and has a better capability of combining calcium and phosphate ions to form apatite on its surface. One of the simplest methods for estimating the surface adhesion properties of materials may be the contact angle. Based on the contact angle, the surface energy of the materials can be obtained. The measured contact angles and calculated surface energies of the four different scaffold materials are shown in Table III. After HA and/or BMP-2 were added to PLLA, the surface energy of the PLLA composite material increased. The highest surface energy was obtained for the PLLA/HA/BMP-2 composite scaffold material. These results illustrate that HA and BMP-2 can enhance the bioactivity of the surface of PLLA fiber membrane materials.

Cell Culture

MTT Assay. The results of the MTT assay tests, after MG63 cells were cultured with PLLA, PLLA/HA, PLLA/BMP-2 and PLLA/HA/BMP-2 for 2, 4, and 6 days, respectively, are shown in Figure 4. The OD value of the four scaffold materials increased with time. However, the OD values of the PLLA/HA/BMP-2 membrane material were significantly higher than the OD values of the PLLA/HA and PLLA/BMP-2 membrane materials (P\0.05, Student's *t* test). This means that the MG63 cells on the PLLA/HA/BMP-2 scaffold material proliferated faster compared with the PLLA/HA or PLLA/BMP-2 scaffold material.

Table III. Comparison of the Contact Angles and Surface Energies Obtained for the Four Different PLLA Scaffold Materials

Specimens	Contact angle (°C)	Surface energy (mN/m)
PLLA	91.3	19.77
PLLA/HA	75.2	28.49
PLLA/BMP-2	69.8	30.27
PLLA/HA/BMP-2	62.7	36.96

SEM Analysis. After the human osteosarcoma cell line, MG63, was cultured on the four different membrane materials for 4 days, the morphology of the MG63 cells on the scaffolds was observed by SEM, and the results are shown in Figure 5. The MG63 cells on the four materials are widely spread and there were also numerous micro-villi and pseudopodia present on all of the membrane materials. On all the scaffold materials where the cells were connected with microvilli and pseudopodia, coverage was complete. This implies that the four materials are biocompatible.

Animal Experiments

Tissue Section Analysis. The histological sections reveal the interface of the materials and the bony tissue. As shown in Figure 6, the inverted micrographs of the pure PLLA scaffold material revealed that, after 30 days, the interface between the material and the host bone was clearly visible and little new bone material had formed around the implant. Nearly the same results were found for the PLLA/HA scaffold material. For the PLLA/BMP-2 scaffold material, the micrograph showed that the interface between the material and the host bone became blurry and a large amount of new bone material was observed. Furthermore, a few new bone tissues had grown into the outer nanofibers of the membrane material. Remarkably, almost no interfaces between the implant materials and the host bone could be identified on the micrograph of the PLLA/HA/BMP-2 scaffold material, suggesting that the new bone tissues already had begun to mineralize. A number of new bone tissues had grown into the implant materials between the inner nanofibers

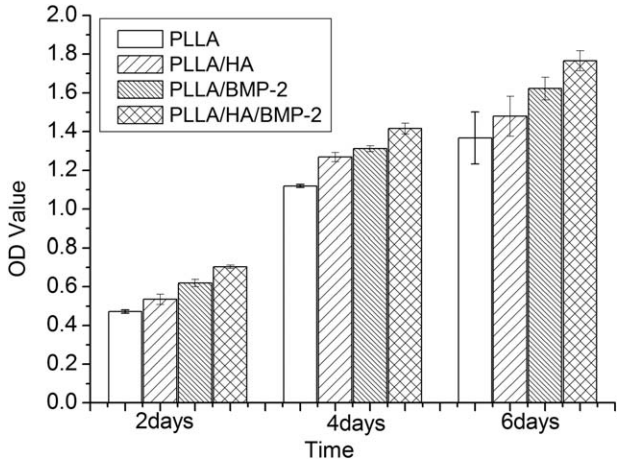

Figure 4. Results of the MTT assay experiments, after MG63 cells were cultured with PLLA, PLLA/HA, PLLA/BMP-2, and PLLA/HA/BMP-2 for 2, 4, and 6 days, respectively.

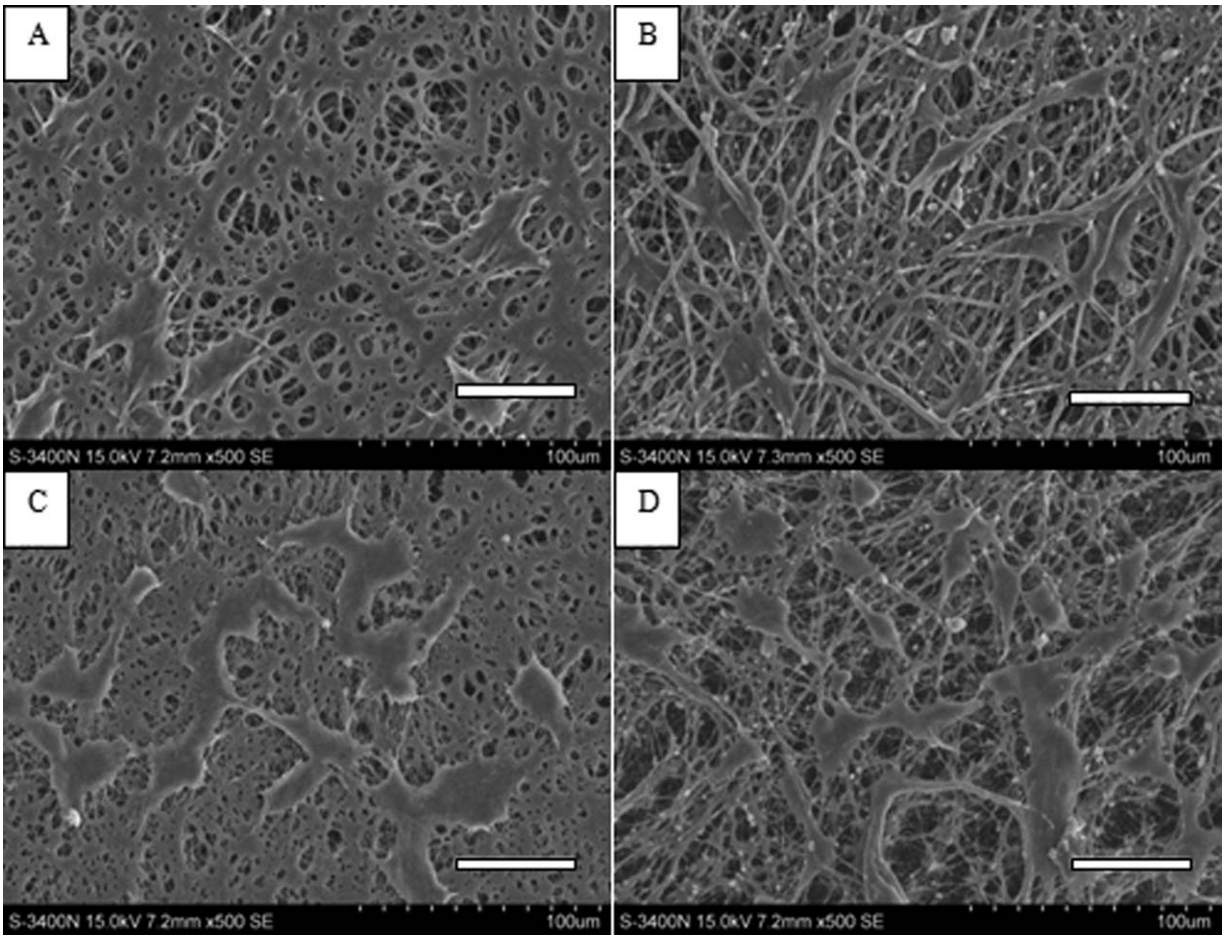

Figure 5. Representative SEM micrographs taken after MG63 cells were cultured on the four different membrane materials for 4 days. (A) PLLA; (B) PLLA/HA; (C) PLLA/BMP-2; (D) PLLA/HA/BMP-2. Scale bar = 50 μm.

in the PLLA/HA/BMP-2 scaffold material. Figure 6G shows that new bone cells had spread all over the implant scaffold.

After 90 days, the new bone tissues had grown further and largely adhered to the implant materials. The new bone material became more and more calcified, resulting in the interfaces between the new bone material and the host bone becoming more blurred. A large amount of the new bone tissue had just grown into the scaffolds. In addition, the photographs showed that, for PLLA, the new bone had just grown into the outer nanofibers, whereas, for PLLA/HA, the new bone material had gradually grown into the inner fibers. In contrast, the new bone material adhered to the nanofibers in the PLLA/BMP-2 scaffold material. Furthermore, the new bone tissue had spread all over the PLLA/HA/BMP-2 scaffold material. With the continuing development and mineralization of the new bone material, the PLLA/HA/BMP-2 scaffold material itself could hardly be identified. These results indicate that the HA and BMP-2 combined with the PLLA scaffold materials played an important role in the growth and calcification of new bone tissue.

DISCUSSION

Results previously published in literature indicated that the surface energy of biomaterials is strongly correlated to its bioactivity, which would affect cell adhesion, proliferation and differentiation. The contact angles and surface energies of the four scaffold materials are compared in Table III. When HA or BMP-2 were added to PLLA, the contact angle of the PLLA/HA and PLLA/BMP-2 was smaller than the contact angle of pure PLLA. The contact angle of the PLLA/HA/BMP-2 composite scaffold material was the smallest among the four scaffold materials, but the surface energy of the PLLA/HA/BMP-2 material was the highest. These results demonstrate that HA and BMP-2 both play an important role in promoting the bioactivity of the PLLA/HA/BMP-2 scaffold material. Furthermore, the results of the MTT assay experiments showed that the OD value of the PLLA/HA/BMP-2 was higher than the OD values of the other three scaffold materials. This implies a better capability of the HA and BMP-2 mixture for improving the bioactivity of nanofiber scaffold materials compared to HA or BMP-2 alone.

It is widely accepted that the bone tissue (re)generation rate serves as an indicator for the bioactivity of the biomaterial. The results of the animal experiments indicate that the amount of new bone tissue in the membrane materials, as well as the tissue between the implants and the host bone, greatly increased with time for the four different scaffold materials. However, after 30 days, the amount of new bone tissue obtained for the PLLA/HA/BMP-2 sample was much higher compared to the other three scaffold materials. After 90 days, the PLLA/HA/BMP-2

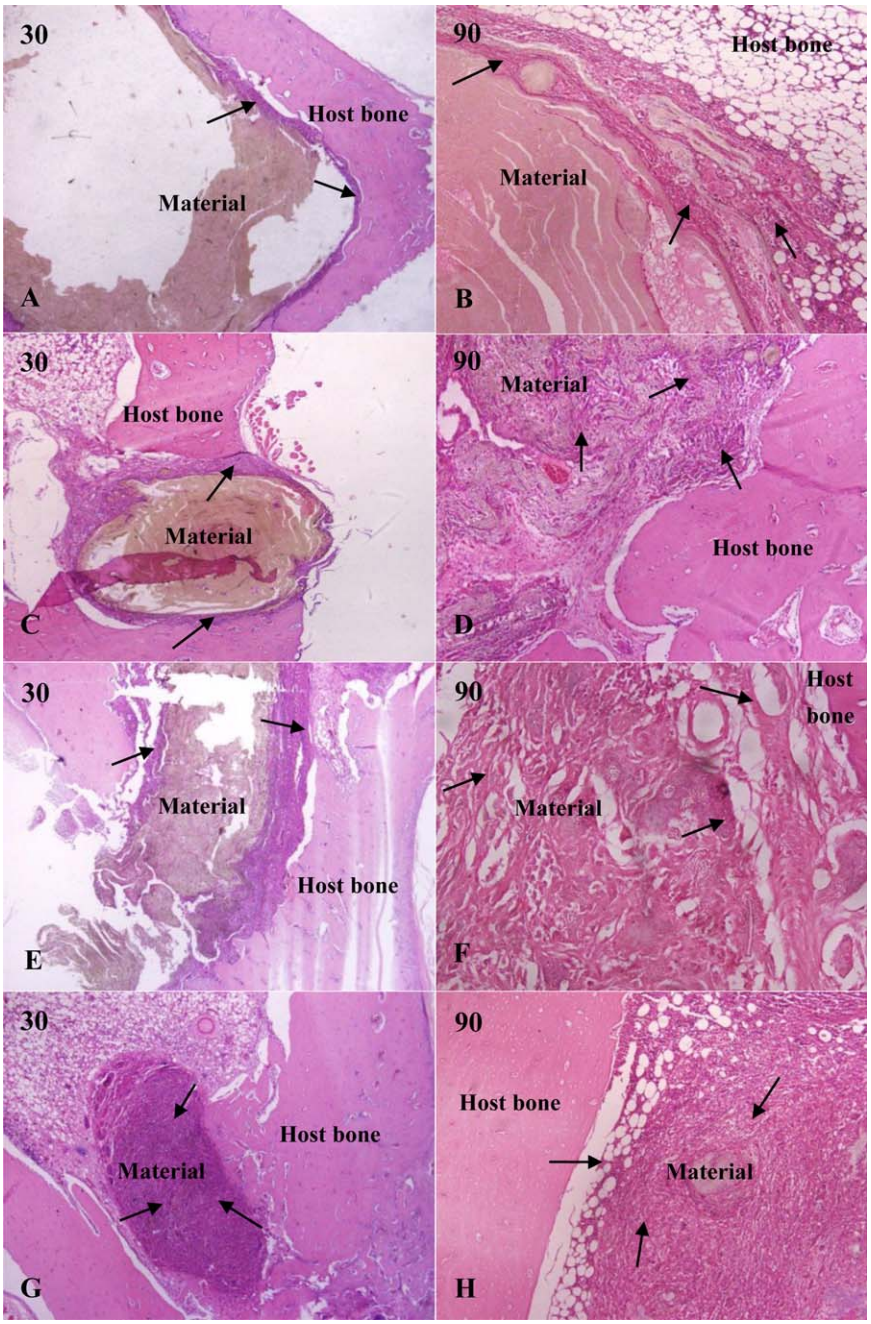

Figure 6. Inverted micrographs of the four different scaffold materials implanted in rabbits for 30 and 90 days, respectively. The arrows point to the newly formed bone material. (A, B) PLLA; (C, D) PLLA/HA; (E, F) PLLA/BMP-2; (G, H) PLLA/HA/BMP-2. [Color figure can be viewed in the online issue, which is available at wileyonlinelibrary.com.]

scaffold material was completely filled with new bone tissue. At the position of the bone defect, there was a large amount of calcium and phosphate ions, and MSCs, implying that, in a real physiological environment, the capability of the PLLA/HA/BMP-2 composite to induce the formation of bone-like apatite by calcium and phosphate ions, to induce MSC to differentiate into osteoblasts, and to promote osteoblast mineralization was much better than the capability of PLLA/HA or PLLA/BMP-2.

CONCLUSIONS

The histological sections and the results of the MTT assay experiments conducted on the four scaffold materials demonstrated that the capability of the PLLA/HA/BMP-2 scaffold material to induce apatite formation, to induce the differentiation of MSCs into osteoblasts, and to promote osteoblast mineralization was better than the capability of the PLLA/HA or PLLA/BMP-2 scaffold materials. It can be assumed that the

PLLA/HA/BMP-2 scaffold material is an excellent material for bone tissue repair.

ACKNOWLEDGMENTS

This research is funded by Chongqing Natural Science Foundation (Grant No. cstc2012jjA10150), Scientific and Technological Research Program of Chongqing Municipal Education Commission (Grant No. KJ130821), the National Natural Science Foundation of China (81000670).

REFERENCES

1. Tang, Y. F.; Liu, J. G.; Wang, Z. L.; Wang, Y.; Cui, L. G.; Chen, X. S. *Chin. J. Polym. Sci.* **2014**, *32*, 805.
2. Schofer, M. D.; Roessler, P. P.; Theisen, C.; Schlimme, S. *PLoS One* **2011**, *6*, 25462.
3. Gao, C. D.; Yang, B.; Hu, H. L.; Liu, J. L.; Shuai, C. J.; Peng, S. P. *Mater. Sci. Eng. C Mater.* **2013**, *33*, 3802.
4. Priddy, L. B.; Chaudhuri, O.; Stevens, H. Y.; Guldberg, R. E. *Acta Biomater.* **2014**, *10*, 4390.
5. Zhi, W.; Zhang, C.; Duan, K.; Liao, G. *J. Biomed. Mater. Res. A* **2014**, *102*, 2491.
6. Karkhaneh, A.; Naghizadeh, Z.; Shokrgozar, M. A.; Bonakdar, S. *J. Appl. Polym. Sci.* **2014**, *131*, 40635.
7. Pan, Z.; Qu, Z. H.; Zhang, Z.; Peng, R.; Yan, C.; Ding, J. D. *Chin. J. Polym. Sci.* **2014**, *31*, 737.
8. Vozzi, G.; Corallo, C.; Daraio, C. *J. Appl. Polym. Sci.* **2013**, *129*, 528.
9. Gao, C.; Gao, Q.; Li, Y.; Rahaman, M. N.; Teramoto, A.; Abe, K. *J. Appl. Polym. Sci.* **2013**, *127*, 2588.
10. Cao, L.; Su, D. F.; Su, Z. Q.; Chen, X. N. *Chin. J. Polym. Sci.* **2014**, *32*, 1167.
11. He, N.; Ke, Q.; Huang, C.; Yang, J.; Guo, Y. *J. Appl. Polym. Sci.* **2014**, *131*, 40404.
12. Chen, L.; Bai, Y.; Liao, G. Y.; Peng, E. J.; Wu, B. L.; Wang, Y. X.; Zeng, X. Y.; Xie, X. L. *PLoS One* **2013**, *8*, 1.
13. Liao, G. Y.; Chen, L.; Zeng, X. Y.; Zhou, X. P.; Xie, X. L.; Peng, E. J.; Ye, Z. Q.; Mai, Y. W. *J. Appl. Polym. Sci.* **2011**, *120*, 2154.
14. Hou, J. Z.; Sun, X. P.; Zhang, W. X.; Li, L. L.; Teng, H. *Chin. J. Polym. Sci.* **2012**, *30*, 916.
15. Liao, G. Y.; Zhou, X. P.; Chen, L.; Zeng, X. Y.; Xie, X. L.; Mai, Y. W. *Compos. Sci. Technol.* **2012**, *72*, 248.
16. Lu, T.; Jiang, M.; Xu, X.; Zhang, S.; Hui, D.; Gou, J.; Zhou, Z. *J. Appl. Polym. Sci.* **2014**, *131*, 41077.
17. Bosetti, M.; Fusaro, L.; Nicoli, E.; Borrone, A.; Aprile, S.; Cannas, M. *J. Biomed. Mater. Res. A* **2014**, *102*, 3531.
18. Abdalla, A. H.; Abdel, S. H.; Felix, B.; Lim, J. H. *Chem. Eng. J.* **2014**, *254*, 612.
19. Ramani, D.; Sastry, T. P. *Cellulose* **2014**, *21*, 3585.
20. Xu, Y.; Zhang, D.; Wang, Z. L.; Gao, Z. T.; Zhang, P. B.; Chen, X. S. *Chin. J. Polym. Sci.* **2011**, *29*, 215.
21. Kim, S. E.; Kim, C. S.; Yun, Y. P.; Jeong, C. M.; Huh, J. B. *Carbohyd. Polym.* **2014**, *114*, 123.
22. Gohil, S. V.; Adams, D. J.; Maye, P.; Rowe, D. W.; Nair, L. S. *J. Biomed. Mater. Res. A* **2014**, *102*, 4568.
23. Wang, D.; Zeng, Q. C.; Song, R.; Meng, X. Z. *BBA Mol. Cell. Res.* **2014**, *1843*, 2744.
24. Qian, X. D.; Zhang, C.; Chen, G. J.; Tang, Z. H.; Liu, Q. W.; Wang, J. F. *Cell Biochem. Biophys.* **2014**, *70*, 1127.
25. Vaz, C. M.; vanTuijl, S.; Bouten, C. V. C.; Baaijens, F. P. T. *Acta Biomater.* **2005**, *1*, 575.
26. Nakamura, M. *J. Ceram. Soc. Jpn.* **2014**, *122*, 755.
27. Yang, J.; Bei, J. Z.; Wang, S. G. *Biomaterials* **2002**, *23*, 2607.